Assessing Intra-Urban Surface Energy Fluxes Using Remotely Sensed ASTER Imagery and Routine Meteorological Data: A Case Study in Indianapolis, U.S.A.

Qihao Weng, *Member, IEEE*, Xuefei Hu, Dale A. Quattrochi, and Hua Liu

***Abstract*—The seasonal and spatial variability of surface heat fluxes is crucial to the understanding of urban heat island phenomenon and dynamics. To estimate energy fluxes, remote sensing derived biophysical variables need to be integrated with surface atmospheric parameters measured in meteorological stations or *in situ* field measurements. In this study, based on the two-source energy balance algorithm, we applied a method to estimate surface energy fluxes by combined use of multispectral ASTER images and routine meteorological data, and applied it to the City of Indianapolis, United States, aiming at in-depth understanding of the spatial patterns of energy fluxes. By computing the fluxes by land use and land cover (LULC) type, we further investigated the spatial variability of heat fluxes. Results show that the energy fluxes possessed a strong seasonality, with the highest net radiation in summer, followed by spring, fall and winter. Sensible heat flux tended to change largely with surface temperature, while latent heat was largely modulated by the change in vegetation abundance and vigor and the accompanying moisture condition. The fluctuation in all heat fluxes tended to be high in the summer months and low in the winter months. Sensible and latent heat fluxes showed a stronger spatial variability than net radiation and ground heat flux. The variations of net radiation among the land use/cover types were mainly attributable to surface albedo and temperature, while the within-class variability in the turbulent heat fluxes was more associated with the changes in vegetation, water bodies, and other surface factors.**

***Index Terms*—Intra-urban variability, seasonality, surface energy fluxes, urban heat island, urban remote sensing.**

I. Introduction

MOST previous urban heat island (UHI) studies have been conducted at the meso-scale using an energy budget approach, which separates the energy flow into measurable interrelated components for simulation modeling. Numerous methods have been proposed and applied, such as *in situ* field measurement, the one-source surface energy balance algorithm (SEBAL), and the two-source energy balance (TSEB) algorithm [1]–[5]. Oke *et al.* [4] obtained the net radiation, sensible, and latent heat flux densities at the roof level by direct measurement. Bastiaanssen *et al.* [1] developed the SEBAL algorithm to independently calculate heat fluxes. Kato and Yamaguchi [2] developed a method to quantify anthropogenic heat discharge as the residue of the energy balance model, and further applied the method to estimate storage heat flux [3]. Timmermans *et al.* [5] compared SEBAL and TSEB, and found that they both contained advantages and disadvantages. The major difference between SEBAL and TSEB lies in whether soil and vegetation are treated separately. For TSEB, heat fluxes are calculated separately for soil and vegetation, while for SEBAL, they are calculated as a composite. A large portion of the Earth's land surfaces are only partially vegetated. Hence, a two-source model can generally estimate the surface energy balance with higher accuracy than a one-source model, especially when the two sources show very different radiometric behavior and atmospheric coupling [5]. The existing literature suggests that there has been a great deal of effort in assessing urban surface energy balance from both observations (e.g., [6], [7]) and from modeling [8]. However, satellite-based assessment of urban energy budgets has received the attention of scientific community less than it deserves, in particular, modeling energy fluxes at the intra-urban scale, in spite of the existence of a few interesting studies (e.g., [2], [3], [9], [10]).

Because the morphological characteristics of urban areas that modify urban climate occur at the micro-scale, it is a great challenge to conduct field studies of energy budget and to understand fully the UHI mechanism without a good understanding of urban morphology. Numerous remote sensing techniques have been developed in support of effective urban sensing of morphological characteristics, detection and monitoring of discrete land use/cover types, and estimation of biophysical variables [11], [12]. In urban climate studies, remotely sensed thermal infrared (TIR) imagery has been used to measure land surface temperature (LST) and emissivity [13]. These measurements provide essential data for analyzing urban thermal landscape pattern and its relationship with surface biophysical characteristics, assessing UHI effect, and relating LST with surface heat fluxes for characterizing landscape properties,

Manuscript received May 26, 2013; revised August 08, 2013; accepted September 03, 2013. Date of publication October 02, 2013; date of current version December 22, 2014. This work was supported by the National Science Foundation under Grant BCS-0521734, and a NASA senior fellowship to Q. Weng. *(Corresponding author: Q. Weng.)*

Q. Weng is with Indiana State University, Terre Haute, IN 47809 USA (e-mail: qweng@indstate.edu).

X. Hu is with the Department of Environmental Health, Emory University, Atlanta, GA 30322 USA (e-mail: xuefei.hu@emory.edu).

D. A. Quattrochi is with the NASA Marshall Space Flight Center, Huntsville, AL 35811 USA (e-mail: dale.quattrochi@nasa.gov).

H. Liu is with the Department of Political Science and Geography, Old Dominion University, Norfolk, VA 23529 USA (e-mail: hxliu@odu.edu).

Color versions of one or more of the figures in this paper are available online at http://ieeexplore.ieee.org.

Digital Object Identifier 10.1109/JSTARS.2013.2281776

patterns, and processes [14]. Through the combined use of TIR and optical sensing data, remote sensing imagery can be used to estimate key surface parameters necessary for estimating surface energy fluxes, which are related to the soil-vegetation system and surface soil moisture, radiation forcing components, and indicators of the surface response to them (i.e., LST) [15]. Previous studies have focused on the methods for estimating variables related to the soil-vegetation system and radiation forcing components, but fewer studies have been done to estimate the surface atmospheric parameters with validation from ground-based meteorological or surface radiation instruments [15]. Estimates of surface energy fluxes using remote sensing have been validated with *in situ* data, but for the most part, have been limited to studies of agricultural or forested landscapes at relatively small spatial scales. For example, Humes *et al.* [16] estimated spatially distributed surface energy fluxes over two small instrumented watersheds in Oklahoma with airborne and satellite-borne data. The model estimates of surface energy fluxes compared well with ground-based measurements of surface flux. Wang and Liang [17] compared MODIS and ASTER data LST and emissivity products with longwave radiation observations during 2000–2007 derived from Surface Radiation Budget Network (SURFRAD) sites. They found that ASTER LSTs had an average bias of 0.1°C, while MODIS LSTs had an average bias of -0.2°C. Examples of other studies that relate remotely sensed surface-atmosphere fluxes (primarily evapotranspiration from instrumented agricultural sites) are provided by Czajkowski *et al.* [18]; Kustas *et al.* [19] and French *et al.* [21]. There is a paucity of studies, however, that have related estimates of surface-atmosphere fluxes derived from satellites with ground-based routine meteorological data in urban areas. Therefore, there is a critical need for integrating the information derived from remote sensing imagery and that from the network of weather stations and/or *in situ* field measurements in modeling urban surface energy fluxes. The urban thermal remote sensing literature is rapidly increasing but works on urban surface energy estimations has not been extended. The majority of previous work [2], [3], [21]–[24] combined satellite measurements with meteorological data to estimate and analyze the spatial patterns of urban heat fluxes based on a one-source surface energy model.

In this study, based on the TSEB algorithm, we applied an analytical protocol to estimate urban surface heat fluxes by combined use of remotely sensed (both optical and TIR) data and routine measurements of a weather station. This method was applied to four Terra's ASTER images of Marion County (the city proper of Indianapolis), Indiana, United States, acquired in different seasons, in order to assess the spatial pattern and its changes in the surface energy balance. By computing heat fluxes by land use and land cover (LULC) type, we further explored the intra-urban variability of the energy fluxes. Finally, we examined how non-surface factors, such as wind speed and aerodynamic parameters, affected the estimation of the heat fluxes.

II. Data and Methodology

A. Study Area and Meteorological Data

Indianapolis, the nation's twelfth largest city, is located on a flat plain of the Midwest. Rapid urbanization is increasing its built-up area through encroachment into the adjacent agricultural, forest, and other non-urban lands. Indianapolis experiences a continental climate. The average July high is 30°C, with the low being 16°C. January highs average 1°C, and lows -8°C. Humidity varies, depending on the position of weather fronts and prevailing winds. Winters may be rather long and cold, with significant snowstorms blowing in from the Great Lakes region. Wind chills can reach into -30°C, with no natural features like mountains to protect the area from the onslaught of arctic Canadian air. Spring and fall bring pleasant air temperatures and the occurrence of many thunderstorms. The city's average annual precipitation is 41 inches (1,040 mm), while snowfall varies from about 20 to 30 inches (500–760 mm) per year (https://climate.agry.purdue.edu/climate/index.asp).

TABLE I
Meteorological Data Used in Estimation of Heat Fluxes

Variable	02/06/06	04/05/04	06/16/01	10/03/00	10/16/06
	1200ET	1200ET	1200ET	1200ET	1200ET
Shortwave radiation (W/m^2)	467	738	895	649	673
Wind Speed (m/s)	4.6	2.6	2.1	2.6	5.7
Atmospheric temperature (K)	266.15	272.15	290.35	288.15	274.15
Air pressure (hPa)	1016.9	1022.7	1020.2	1014.9	1009.8
Relative humidity (%)	92	63	86	93	74

The ground meteorological data needed to calculate heat fluxes include solar radiation, air temperature, relative humidity, air pressure, and wind speed. The solar radiation data was acquired from the National Climatic Data Center (NCDC), which supplied hourly modeled solar radiation data along with hourly meteorological data between 1991 and 2005 from the National Solar Radiation Database (NSRDB). An earlier version of the database was also available for the Indianapolis Airport station covering 1961–1990. Since the shortwave radiation changes with date and time, we selected the shortwave radiation value modeled for the same day as the image acquisition date and at the closest matching time between the NSRDB measurement and the satellite overpass. The data for air temperature, relative humidity, air pressure, and wind speed were obtained from Indiana State Climate Office and NCDC. The stations reporting to NCDC provided hourly measurements for these routine parameters in addition to precipitation and other weather conditions. The meteorological data measured at the time closest to each satellite overpass were used in this study. The meteorological parameters were assumed constant throughout the study area. Since the study area is flat, air temperature was not corrected for differences in elevation. The precipitation records were checked prior to each satellite overpass to understand the moisture conditions over land surfaces. The meteorological data used in the study are shown in Table I.

B. Remote Sensing Data Acquisition and Pre-Processing

ASTER images of Marion County, Indiana, acquired on October 03, 2000 (12:00:51 eastern standard time, the fall image), June 16, 2001 (11:55:29, the summer image), April 05, 2004 (11:46:39, the spring image), and February 06, 2006 (11:45:36,

the winter image) were used to study seasonal changes in surface heat fluxes. Additionally, an ASTER image of October 13, 2006 (11:40:01) was acquired for comparison with the October 3, 2000 image to examine the impact of non-surface factors on the estimation of heat flux. The ASTER data products including surface kinetic temperature, surface spectral emissivity, VNIR (visible and near infrared) and SWIR (short-wave infrared) surface spectral radiance were obtained from NASA. The methodology for converting ASTER infrared measurements to LSTs has been reported by Gillespie *et al.* [25]. We used the ASTER data products of the VNIR and SWIR spectral radiance to calculate the spectral reflectance. Surface spectral reflectance and spectral emissivity data were converted into surface albedo and broad-band emissivity according to Liang [26] and Ogawa *et al.* [27] respectively.

All ASTER images were re-sampled to 90-meter resolution to correspond to the spatial resolution of their TIR bands. By resampling up from 15 m to 90 m, the radiometry of original reflective bands will be preserved, and the process will not introduce autocorrelation in the resultant data. NDVI was calculated using atmospherically corrected at-surface reflectance of Near IR band and red band of TM data. Linear Spectral Mixture Analysis (LSMA) was applied to derive fractional images. Details about the selection of end-members and the estimation of the vegetation fraction (denoted as f_v in this study) were discussed in Weng *et al.* [28]. The non-vegetation fraction (denoted as f_{nv}) was calculated as: $1 - f_v$.

With ASTER VNIR and SWIR bands, six LULC types were identified by employing an unsupervised classification algorithm, i.e., Iterative Self-Organizing Data Analysis [29]. Fig. 1 shows the resultant classified LULC maps. The overall classification accuracy of 92% (April 5, 2004, image), 88.33% (June 16, 2001, image), 87% (Oct. 3, 2002, image), 87.33% (February 6, 2006, image), 89% (Oct. 13, 2006, image) was achieved respectively [29]. A comparison among the five classified maps indicates that the magnitude and spatial pattern of each class corresponded well to each other but also reflected the seasonal and temporal differences [29].

C. Estimating Surface Heat Fluxes

1) Net Radiation (R_n): The net radiation was calculated as follows:

$$R_n = (1-\alpha)R_{short} + \varepsilon\varepsilon_a\sigma T_a^4 - \varepsilon\sigma T_s^4. \tag{1}$$

Where R_n is the net radiation, σ ($= 5.67 \times 10^{-8}$ W/m^{2}K^4) is the Stefan-Boltzmann constant, ε_a is atmospheric emissivity, α is broadband albedo, R_{short} is short wave radiation, ε is surface broadband emissivity (that is assumed to be equivalent to the absorptance of the downward long wave radiation), T_a is atmospheric temperature, and T_s is surface temperature [5].

Atmospheric emissivity (ε_a) was calculated as:

$$\varepsilon_a = 1.24\left(\frac{e_a}{T_a}\right)^{1/7} \tag{2}$$

where e_a is atmospheric water vapor pressure, which was estimated based on saturation water vapor pressure e^* and relative humidity [30].

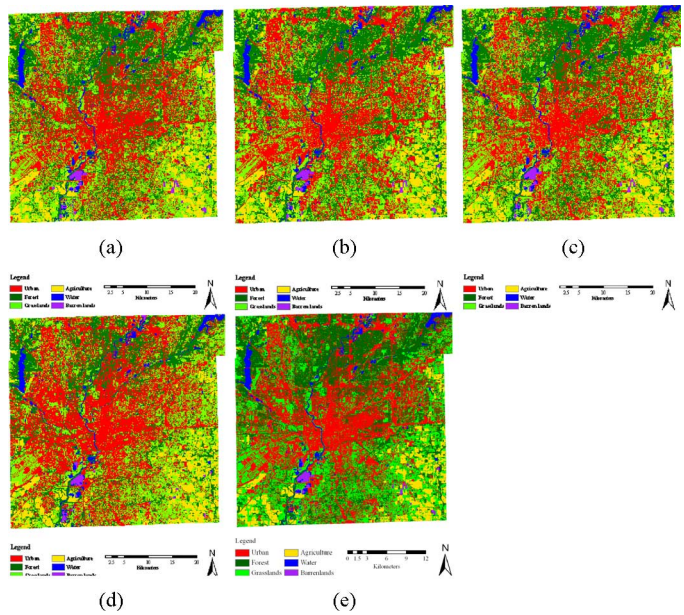

Fig. 1. Land use and cover classification maps of Indianapolis, U.S.A., on five dates. From upper left to lower right: (a) April 5, 2004; (b) June 16, 2001; (c) October 3, 2000; (d) February 6, 2006; and (e) October 13, 2006.

Surface reflectance can be calculated using the following equation:

$$\rho = \frac{\pi * (L_{sat} - L_{haze}) * d^2}{Esun_\lambda \left[(\cos\theta_s)^2\right]} \tag{3}$$

where: ρ is surface reflectance, L_{sat} is at-sensor radiance, d is the earth-sun distance, $Esun_\lambda$ is a band-dependent constant, θ_s is the solar zenith angle, and L_{haze} is estimated upwelling scattered path radiance due to atmospheric haze, aerosols, etc. [31]. After the surface reflectance was calculated, the broadband albedo α can be calculated using the method developed by Liang [27]. Broadband emissivity (ε) was calculated based on the spectral emissivities of all bands [28].

2) Ground Heat Flux (G): Estimation of ground heat flux, G, is often difficult, since it requires knowledge of the temperature gradient in the soil [15]. In urban areas, the heat conductivity of land surface materials and the vertical temperature gradient inside the walls, roofs, and floors for buildings must also be known [2]. In practice, the information is hardly obtainable. Therefore, the ground heat flux is largely estimated based on the net radiation as:

$$G = c_g * R_n. \tag{4}$$

The coefficient, c_g, is subject to the influence of surface cover material and seasonality ([32], [33]), as well as diurnal change [34]. Given the heterogeneity and complexity of urban component surfaces, Grimmond *et al.* [35] proposed the objective hysteresis model and tested it in Vancouver; this calculated G as a function of continuously measured net radiation and the surface properties of the site. Since remote sensing measurements are instantaneous in time, we had to use a look-up table for c_g, which was compiled by Kato and Yamaguchi [2] and

TABLE II
PARAMETERS USED FOR ESTIMATION OF HEAT FLUXES

LULC Type	C_g	d_0 (m)	Z_{0m} (m)	Z_{0h} (m)
Water	0.35	0.05	0.00003	0.000088
Bare soils	0.3	0.05	0.001	0.00002
Grass	0.3	0.1	0.1	0.001
Forest	0.15	1.5	0.3	0.0003
Urban	0.4	1.95	0.33	0.0033
Agriculture	0.3	0.1	0.1	0.001

Note:
C_g: coefficient for estimating ground heat flux [2];
Z_{0m} and Z_{0h}: Roughness lengths for momentum and heat transport Kato and Yamaguchi, 2005; and
d_0: Displacement height for different land cover types [44].
The aerodynamic parameters (d_0, Z_{0m} and Z_{0h}) for the urban category were determined based on a research result by Burian *et al.* (2003) who computed the displacement height for the city of Houston, Texas for a project on urban building databases funded by U.S. Environmental Protection Agency.

was mainly based on the findings of Anandakumar [32]. Table II shows assigned c_g values based on LULC type.

3) Sensible Heat Flux (H): The sensible heat flux was calculated as:

$$H = f_{nv} H_{non-veg} + f_v H_{veg} \tag{5}$$

where $H_{non-veg}$ and H_{veg} are sensible heat flux for non-vegetated and vegetated areas, respectively. $H_{non-veg}$ and H_{veg} were calculated using the following equations:

$$H_{non-veg} = \rho_a c_p \frac{T_s - T_a}{R_{AH} + R_s} \tag{6}$$

$$H_{veg} = \rho_a c_p \frac{T_c - T_a}{R_{AH}}. \tag{7}$$

Where ρ_a is the air density in $\mathrm{kg/m^3}$, C_p is the specific heat of air at constant pressure in $\mathrm{J/(kg \cdot K)}$, T_s and T_c are surface temperatures for non-vegetated and vegetated areas, respectively (both were obtained from the ASTER kinetic surface temperature product), T_a is atmospheric temperature, R_{AH} is the aerodynamic resistance in s/m, and R_s is the resistance to heat flow in the boundary layer immediately above the soil surface [36]. R_{AH} was calculated as:

$$R_{AH} = \frac{\left[\ln\left(\frac{z_u - d_0}{z_{0M}}\right) - \Psi_M\right]\left[\ln\left(\frac{z_t - d_0}{z_{0H}}\right) - \Psi_H\right]}{k^2 u}. \tag{8}$$

Where z_u ($= 10$ m) and z_t ($= 2$ m) are the respective heights at which the wind speed u and atmospheric temperature are measured, d_0 is the displacement height, and z_{0M} and z_{0H} are the roughness lengths for momentum and heat transport, respectively. All measurements are in meters. In addition, Ψ_M and Ψ_H are stability correction functions for momentum and heat, and k ($= 0.4$) is von Karman's constant [30]. The (8) may be simplified by removing Ψ_M and Ψ_H [37]. Table II shows that the values of d_0, z_{0m} and z_{0h} were fixed according to each LULC type and were estimated based on the existing literatures.

R_s can be computed per the following equation:

$$R_s = \frac{1}{a + bu_S}. \tag{9}$$

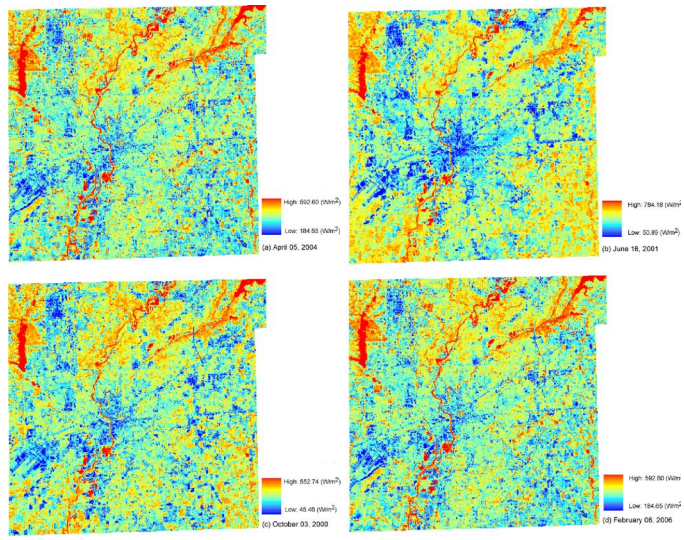

Fig. 2. Net radiation in Indianapolis, U.S.A. on April 5, 2004, June 16, 2001, October 3, 2000, and February 6, 2006.

Where a ($= 0.004$ m/s) is the free convective velocity, b ($= 0.012$) is a coefficient to represent the typical soil surface roughness, u_s is the wind speed over soil surface at the height of 0.05-0.2 m [36].

4) Latent Heat Flux (LE): Latent heat flux was calculated following [38]:

$$LE = f_{nv} LE_{non-veg} + f_v LE_{veg}. \tag{10}$$

$LE_{non-veg}$ and LE_{veg} are latent heat flux for the non-vegetated and the vegetated areas, respectively. They were computed as follows:

$$LE_{non-veg} = R_{N,S} - G - H_{non-veg} \tag{11}$$

$$LE_{veg} = \alpha_{PT} f_{\mathrm{G}} \frac{\Delta}{\Delta + \gamma} R_{N,C} \tag{12}$$

where α_{PT} ($= 1.26$) is Priestley-Taylor parameter, γ is psychrometric constant, Δ is the slope of saturation vapor pressure – temperature curve, f_{G} (equals unity if not available) is the fraction of the LAI that is green. $R_{N,S}$ and $R_{N,C}$ are net radiation for soil and vegetation, respectively [36]. If a negative value of $LE_{non-veg}$ was obtained, it would be set equal to zero. $H_{non-veg}$ was then recomputed as the residual of (11) when $LE_{non-veg}$ was set to 0 and $R_{N,S}$ and G are from previous calculations [38].

III. RESULTS

A. Heat Fluxes in the Four Imaged Dates

Figs. 2–5 show estimated net radiation, sensible heat flux, latent heat flux, and ground heat flux in four seasons. The mean values and standard deviations of the surface heat fluxes are displayed in Table III.

The mean value of net radiation was 432 in April, 613 $\mathrm{W/m^2}$ in June, 403 $\mathrm{W/m^2}$ in October, and 319 $\mathrm{W/m^2}$ in February, respectively. The result indicated that the highest net radiation was received in summer, followed by spring, fall and winter, a typical seasonal pattern in the mid-latitude region in the northern

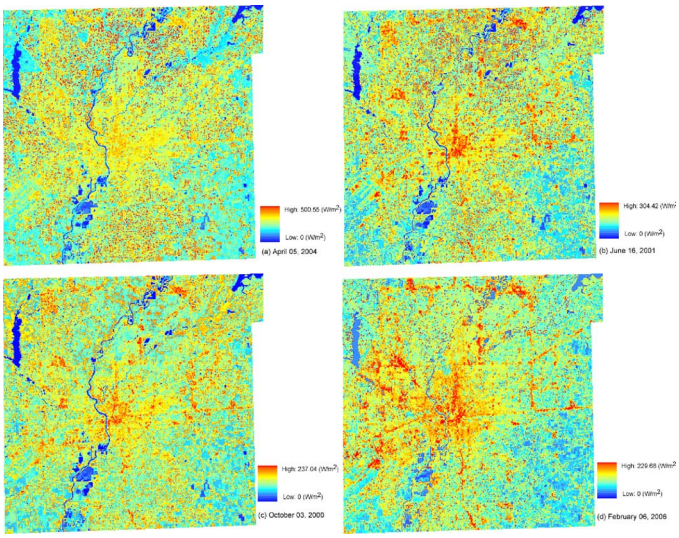

Fig. 3. Sensible heat flux in Indianapolis, U.S.A. on April 5, 2004, June 16, 2001, October 3, 2000, and February 6, 2006.

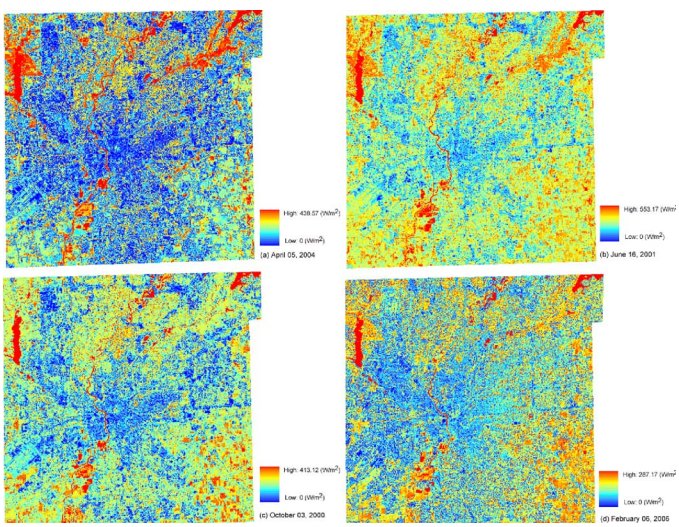

Fig. 4. Latent heat flux in Indianapolis, U.S.A. on April 5, 2004, June 16, 2001, October 3, 2000, and February 6, 2006.

hemisphere. This was due primarily to different amounts of solar (shortwave) radiation received by the Earth surface. Moreover, the amount and vigor of vegetation varied significantly in different seasons in Indiana, and different amounts of vegetation can significantly affect net radiation. The ground heat flux showed a similar seasonal pattern because G was estimated from R_n. The standard deviation of net radiation was the highest in summer and the lowest in winter, which was, again, affected by the vegetation pattern. The vegetation was the most heterogeneous during the summer as a result of various species, life forms, structures and habitats, and was the least during the winter since most vegetation were dead. The standard deviation of R_n was higher in the spring than in the fall. In the mid-latitude region, phenological changes were more obvious in the spring than in any other seasons.

In terms of sensible heat flux, values of 165, 128, 117, and 93 $\mathrm{W/m^2}$ were obtained for each imaging date in April, June, October, and February, respectively. Sensible heat flux is driven

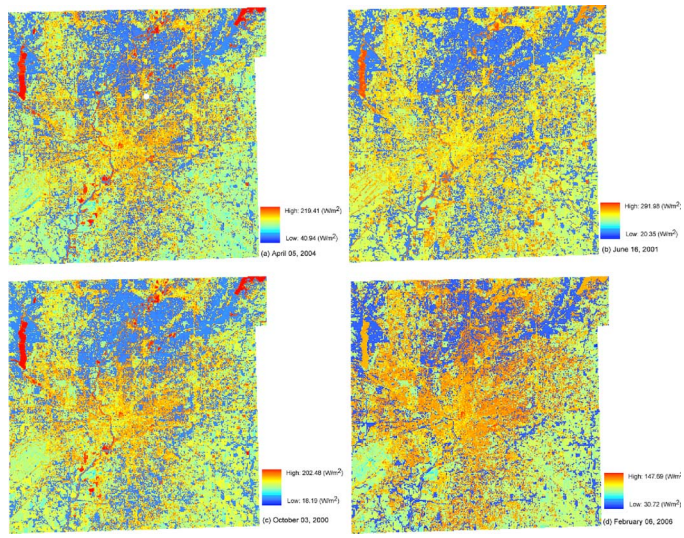

Fig. 5. Ground heat flux in Indianapolis, U.S.A. on April 5, 2004, June 16, 2001, October 3, 2000, and February 6, 2006.

TABLE III
MEAN AND STANDARD DEVIATION VALUES (IN PARENTHESIS) OF HEAT FLUXES IN FOUR DATES

Heat Flux ($\mathrm{W/m^2}$)	04/05/2004	06/16/2001	10/03/2000	02/06/2006
Net Radiation (R_n)	432 (41)	613 (48)	403 (40)	319 (18)
Sensible Heat Flux (H)	165 (71)	128 (56)	117 (47)	93 (38)
Latent Heat Flux (LE)	104 (89)	195 (94)	101 (66)	96 (62)
Ground Heat Flux (G)	124 (39)	176 (56)	114 (37)	97 (30)

by temperature differences between the atmosphere and the surface and as such is highly variable in space and in time. Its seasonal variability was obvious based on our result. It showed the highest H in the spring. The extreme low atmospheric temperature ($-1\mathrm{C}^\circ$) and larger wind speed at the time when the April image was acquired were two main factors contributing to this anomaly. LULC change associated with urban sprawl between 2000 and 2004 may be another factor. The urbanization process favored higher sensible heat flux as evapotranspirative surfaces were reduced. Moreover, increased anthropogenic heat discharges also contributed to the sensible heat flux. The spatial variation in H was high in the summer months but was generally low in the winter months. From April to October in Indiana (the summer months), there were a larger amount of vegetation and more growth-related activities, and also a bigger contrast among the urban, suburban and rural areas in radiative, thermal, moisture, and aerodynamic properties. In comparison with net radiation, sensible heat flux showed a stronger spatial variability (thus higher standard deviation) in all imaging dates. Although there were a variety of surface materials and seasonal changes in vegetation amount and vigor, which affected surface albedo and emissivity, the differences in the net shortwave and longwave radiation were constrained by the albedo-temperature feedback mechanism [22], [39].

The latent heat flux showed an obvious seasonal variability too. LE value yielded 104 $\mathrm{W/m^2}$ in April, 195 $\mathrm{W/m^2}$ in June,

101 $\mathrm{W/m^2}$ in October, and 96 $\mathrm{W/m^2}$ in February. The decrease of LE value was attributed to the change in vegetation transpiration and water evaporation, reflecting the vegetation growth and decline over a year cycle and the accompanying moisture condition by season. The highest LE value corresponded to the existence of the largest amount of vegetation and its vigor in the summer. LE reached the lowest point in February. The standard deviation value of LE, again, was the lowest in the winter due to a less contrasting surface condition in terms of evapotranspiration. It should be noted that LE had a stronger variability in the spring time (standard deviation: 89) than in the fall (standard deviation: 66), as various species of vegetation and crops started to grow following different calendars. This variability contributed to a higher standard deviation value in spring, and was closely related to the spatial pattern of LE.

B. Heat Fluxes by LULC Type

Fig. 6 shows the mean and standard deviation values of each flux by LULC type. It is clear that in all dates water exhibited the highest R_n, followed by forest. The lowest R_n values were detected in urban in the summer months while in bare soil in the winter months. Agriculture and grass land possessed the third and fourth places. The variations of R_n were only controlled by surface albedo and surface temperature. Water bodies generally had low albedo and surface temperature resulting in a high R_n. Forest yielded a high R_n value as a consequence of its ability of absorbing more solar energy, lowering albedo and temperature. Owing to the higher surface temperature, the long-wave upward radiation from the urban surfaces was higher, and thus urban areas often discovered the lower R_n than the nearby rural areas. However, the lowest R_n position can be overtaken by bare soil in the winter months (in February and April) because of its high albedo. Bare grounds may be covered by snow and were frequently seen in dry and plowed conditions in the early spring before planting. Agriculture and grassland emulated closely in both mean and standard deviation values of R_n, followed by their similar cover conditions in albedo and surface temperature. The variability of R_n was relatively high in bare soil, water, and urban, especially in the summer. High variability of net radiation over water (especially the two reservoirs in the study areas) may be associated with the growth of algae. But the fluctuation became much weaker in the winter (February image). The fall and spring images shared similar moderate variability in R_n.

The estimation of sensible heat flux was found to be linked with surface temperature. Urban possessed the highest H values due to higher surface temperature and surface roughness. Various types of impervious surfaces generally produced higher thermal emittance into the atmosphere as sensible heat. Moreover, anthropogenic heat discharge in the urban areas was much higher than in the rural, which contributed substantially to the sensible heat flux, especially in the winter months. In contrast, water yielded the lowest H. The contrast of H between urban and water was most pronounced in the spring and summer, but became less obvious in the fall, reaching the lowest in the winter. It is abnormal to learn that both forest and grass displayed a high H, regardless of the seasonality. We believe that the fact that forest and grass were mingled with urban in the study area had caused image misclassification. Forest was mostly confused with residential land (especially in the low-density and medium density areas), which in our classification scheme belonged to urban. Grass was largely found in the residential areas, confusing itself with urban too. Another interesting finding was that bare soil always exhibited a low H, preceded only by water. Geographically, bare soil was largely located along rivers and other water bodies with small amount scattered within agricultural land (see Fig. 1). The spatial adjacency between soil and water/ agricultural land may have caused mis-classification and have thus resulted in computation error in the estimation of H for bare soil. The standard deviation values were high in forest, grass and urban, but all decreased to the lowest in the winter.

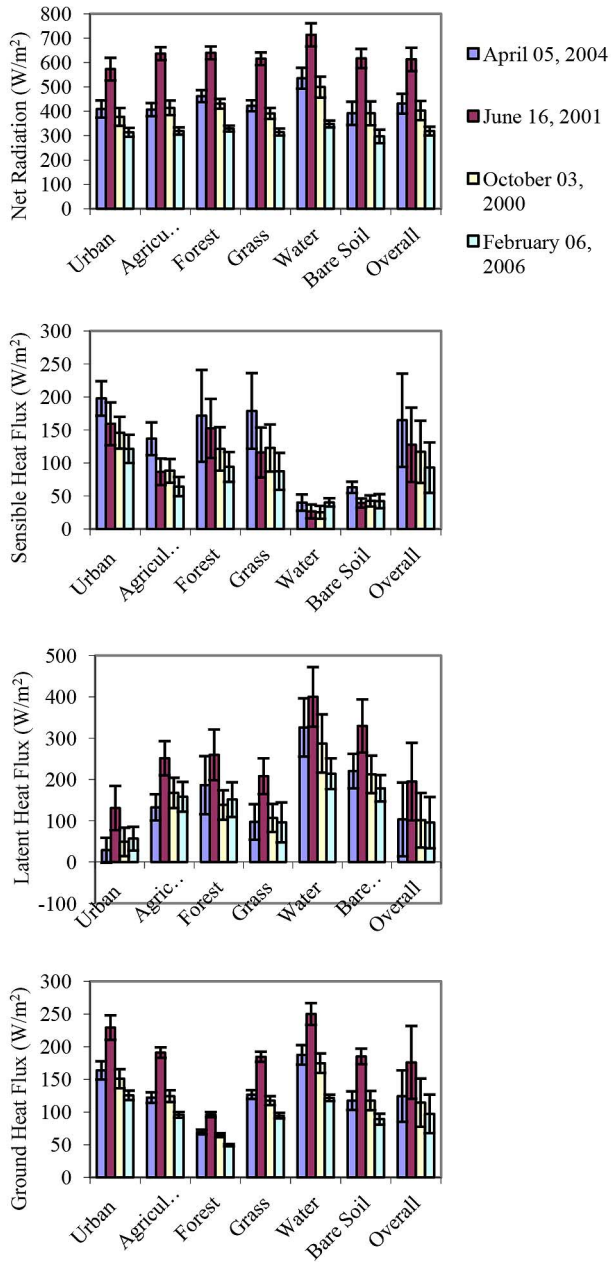

Fig. 6. A comparison of mean and standard deviation values of heat fluxes on four dates.

Because latent heat flux was associated with evapotranspiration, it becomes apparent from Fig. 6 that high LE corresponded to water, agriculture, and forest. Grass also displayed fairly high LE in the summer, but declined to considerably low levels in other months. At all times, urban possessed the lowest LE, but a large standard deviation value. This strong intra-class variability can be largely attributed to the image classification scheme, where residential lands were combined with commercial, industrial, and transportation etc. to form the urban class. The increase of the standard deviation in LE was related to the change of vegetation abundance and vigor within the urban class, especially in the residential areas. It is worthy to note that bare soil detected the second highest LE in all four dates. This over-estimation was mainly caused by image misclassification between bare soil and water and its confusion with agriculture, forest, and grass. Overall, since the fluctuation of LE had much to do with precipitation and vegetation activities, the standard deviation values for all LULC types appeared to be high from April to October. By comparing standard deviation values among all the heat fluxes for all LULC types, it is apparent that both LE and H generated a strong variability in the four imaging dates, while R_n and G observed a relatively weak variability.

C. Influences of Aerodynamic Parameters

Surface energy processes across the soil – vegetation – atmosphere continuum are turbulent processes involving heat, water and momentum exchange at a surface; and thus the estimation of heat fluxes are often based on the vertical gradients of temperature, water vapor and wind speed above the surface using flux-gradient relationships [40]. Campbell and Norman [41] suggested that those processes are related to soil moisture, canopy structure, land cover, topography, and surface albedo. It has been further suggested that the surface energy balance is also depended upon surface roughness (e.g., [23]), typically characterized by two aerodynamic parameters, aerodynamic roughness length and displacement height. The term, R_{AH}, is a rather complex function of various geometric factors, including roughness lengths, displacement height, and the wind speed, and is often empirically estimated [15], [42]). In determining R_{AH}, this study followed the works of Brutsaert [30], Kato and Yamaguchi [2], and Liu *et al.* [37]. Since the last two sections have focused on discussion of surface factors (e.g., land cover, vegetation activities and abundance, surface albedo etc.) for energy modeling, this section examined the effects of "non-surface" factors on the surface energy balance. Special attention would be paid to the issue of how aerodynamic parameters (displacement height and roughness length for momentum) and wind speed may influence the estimation of heat fluxes.

The result of radiometric correction between the October 3, 2000 image and the October 13, 2006 images indicated that all regression equations were significant at the 0.001 level and yielded a R^2 value above 0.8 for most bands. Since a relative radiometric correction was conducted between these two near-anniversary images, the changes in the thermal pattern should largely be attributed to the "surface" factors and local aerodynamic parameters. The former was related to the thermal properties of surface materials, the composition and layout of LULC types, and anthropogenic effects. By comparing with the LULC maps on these two dates (Fig. 1(c) and (e)), it becomes clear that that the percentage of each LULC type had remained relatively stable. To evaluate the effect of the LULC changes on the estimation of the surface heat fluxes, the mean and standard deviation values per LULC type were compared (Table IV). The result indicated that while R_n and G had not changed significantly, H increased and LE decreased substantially. The changes in H and LE values and their spatial variabilities cannot be attributed to the LULC changes between 2000 and 2006, which were considered insignificant in respect to magnitude as well as to the spatial pattern (location and geometry). An inquiry into the abnormal high H flux suggested that the extremely high wind speed (5.7 m/s) on October 16, 2006 was probably the main cause. The wind speed was 2.6 m/s on October 3, 2000. Moreover, the atmospheric temperature and the mean LST for the study area were 274.15 K and 286.89 K on October 16, 2006, and 288.15 K and 301.5 K on October 3, 2000, respectively. The difference in the vertical gradient of temperature was not notable. Since $LE_{non-veg}$ was estimated as the residue of the heat balance equation ((11)), a high H had resulted in a low LE value.

TABLE IV
A COMPARISON OF THE HEAT FLUX STATISTICS BETWEEN OCT. 3, 2000 AND OCT. 16, 2006 (UNIT: W/m^2)

Heat flux	Year	Overall			Urban	Agri.	Forest	Grass	Water	Bare Soil
		Mean (stad. dev.)	*Range*	*Ratio to R_n*						
Net Radiation	2000	403 (40)	295-553		377 (36)	414 (30)	431 (20)	391 (23)	499 (43)	392 (49)
	2006	396 (41)	260-536		378 (41)	395 (33)	426 (20)	379 (26)	484 (29)	364 (57)
Sensible Heat Flux	2000	117 (47)	0-241	0.3	146 (24)	88 (18)	121 (33)	123 (36)	25 (10)	43 (8)
	2006	249 (105)	0-480	0.63	311 (44)	183 (32)	274 (99)	244 (73)	77 (12)	91 (15)
Latent Heat Flux	2000	101 (66)	0-245	0.25	49 (34)	168 (37)	138 (36)	107 (34)	287 (70)	212 (46)
	2006	39 (52)	0-300	0.1	0.7 (8)	66 (40)	62 (35)	40 (37)	232 (53)	150 (49)
Soil Heat Flux	2000	114 (37)	55-202	0.28	151 (15)	124 (9)	65 (3)	117 (7)	175 (15)	117 (15)
	2006	113 (37)	53-182	0.28	151 (16)	119 (10)	64 (3)	114 (8)	170 (10)	109 (17)

Another important parameter is displacement height, d_0. It can be roughly conceptualized as the height of a surface formed by distributing the aggregate volume of roughness elements and their wake re-circulation cavities uniformly over the underlying surface [43]. We defined d_0 for each surface type based on Kustas *et al.* [44], except for the urban class. The d_0 for the urban category was a modification of the result by Burian *et al.* [45] who computed it for the city of Houston, Texas, in a project on the development of urban building databases. Burian *et al.* [45] compared three methods of calculation for d_0, proposed by Grimmond and Oke [46], Raupach [47], and Macdonald *et al.* [43] respectively, and computed it by using each method for the entire study area of 1,653 km^2 centered on the downtown Houston. They further computed d_0 for each LULC type using standard morphometric equations and the derived urban morphological parameters. In our estimate, we considered the differences in urban building and vegetation morphology between Houston and Indianapolis and in the LULC classification

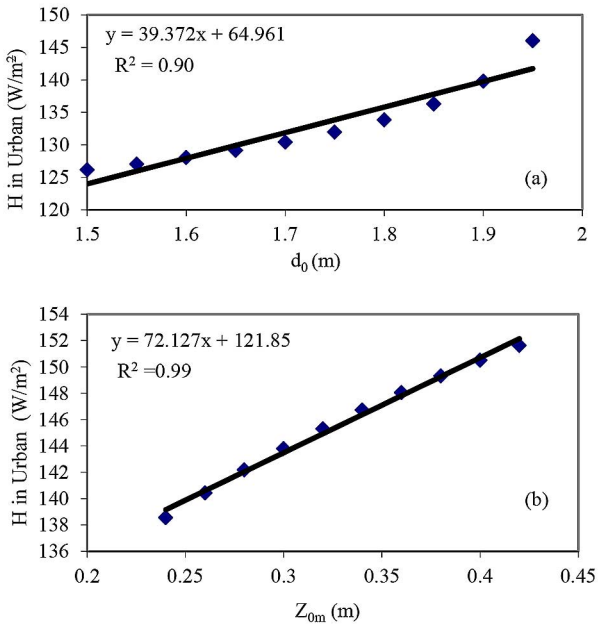

Fig. 7. Sensitivity analysis of urban aerodynamic parameters. (a) Sensible heat flux as a function of displacement height (d_0) in the urban areas; (b) Sensible heat flux a s a function of roughness length for momentum (Z_{0m}) in the urban areas.

schemes. To examine the effect of d_0 on H in the urban areas, we conducted a sensitivity analysis. The value of d_0 was chosen in the range of 1.5 to 1.95 m with an increment of 0.05. This selection mainly considered the result of Burian *et al.* [45], in which a table was compiled to provide d_0 and Z_{0m} values for US cities of various urban morphological characteristics. Although the city of Indianapolis was not included in that table, however, the table provided a valuable reference in determining the range of d_0. For each d_0, H value for the urban class was re-computed while holding Z_{0m} $(= 0.33)$ and Z_{0h} $(= 0.00033)$ to be constant. The October 3, 2000 image was used for the sensitivity analysis. Fig. 7(a) shows the result of regression analysis. The relationship between H and d_0 is almost linear, with a R^2 value of 0.9. For any increase of 0.1 m in d_0, urban H would increase by approximately 3.94 $\mathrm{W/m^2}$. Obviously, the influence of displacement height in the urban areas can be large. A proper value of d_0 should be derived based on a detailed study of urban morphology using remotely sensed data and *in situ* field survey. Equally important is a reliable urban LULC classification based on the remote sensing data characteristics. With our TSEB method, d_0 may also have a moderate impact on the estimation of LE in the urban areas.

In this study, roughness lengths Z_{0M} and Z_{0H} were defined as a function of LULC type. The estimations by Burian *et al.* [45] and Kato and Yamaguchi [2] were modified for use in this study, which considered the differences in LULC classification and in urban morphology between their studies and the present study. Our sensitivity analysis focused on the influence of Z_{0M} in the urban areas on H. Since Z_{0M} had been evaluated in various field campaigns but Z_{0H} had not [46], we thus determined to estimate Z_{0H} assuming that it possessed a fixed relationship with Z_{0M}. Sensible heat flux H in the urban areas was computed by increasing Z_{0H} by 0.02 m for each test in the range of 0.24 to 0.42 m. The d_0 was kept at 1.95 m at all times. Fig. 7(b) shows a nearly linear relationship between H and Z_{0H}, with a R^2 value of 0.99. For an increase of 0.1 m in Z_{0H}, urban H would increase by approximately 7.21 $\mathrm{W/m^2}$, nearly two times larger than that of d_0. The influence of Z_{0H} was apparently larger than d_0 on urban sensible heat. A thorough study and detailed measurement for this parameter is warranted for both future urban climate and remote sensing studies.

D. Result Comparison

The validation of heat fluxes would be ideal if *in situ* field measurements were available for the study area; although the existing literature has warned that special attention should be directed towards a better understanding of the differences between modeled and measured fluxes [48]. Due to the lack of field measured data in the study area, we chose to compare our result with that of Kato and Yamaguchi [3], which had been verified with *in situ* field measurements. The two study areas were located in the similar latitudes: Indianapolis has latitude of 39°47'N at its geometry center and Nagoya, Japan, 35°10'N. Both cities are in a temperate climate zone, but Indianapolis is more continental than Nagoya. They had similar surface cover conditions too, but Indianapolis had more vegetation than Nagoya. Table V shows that two pairs of images were chosen for comparison, one in the winter (the February 6, 2006 image of present study *vs*. the January 2, 2004 image of Kato and Yamaguchi) and the other in summer (the June 16, 2001 of present study *vs*. the July 10, 2000 image of Kato and Yamaguchi). It is worthy to note that these images were acquired at similar times during a day, i.e., around noon time.

Table V indicates that the ranges of estimated heat fluxes in this study were largely in agreement with those of Kato and Yamaguchi. Our LE values were estimated to be higher. The difference in LE prompted us to examine the differences in the computation algorithms. We applied a TSEB modeling algorithm, while Kato and Yamaguchi utilized a one-source surface energy balance method. A two-source approach should yield more realistic values for sensible heat flux over sparsely vegetated and dry areas (as a city is). Under these conditions a single source approach generally under-estimates the sensible heat fluxes, and thus over-estimates the latent heat fluxes. Therefore the algorithm used most probably is not the reason for finding higher latent heat fluxes here; they should be lower as a consequence of the two-source method. Kato and Yamaguchi [3] assumed that there was not any latent heat in the urban areas, which may be the main reason why in the current study higher LE values were found. In order to have a better comparison of the energy balance in the two study areas, the relative ratios of H, LE, and $G(\Delta G)$ to R_n for chosen LULC types were compared. The H/R_n ratio of the present study appeared to be higher than their study in the urban class, especially in the winter. This difference had much to do with the mis-matched LULC classifications between the two studies. Our "urban" class included commercial, industrial, transportation, and residential, whereas their study separated urban and residential in computing the H/R_n ratio. In contrast, our "agriculture" category matched well with their "field" class, both yielding a ratio of 0.14.

TABLE V
RANGES OF HEAT FLUXES AND THEIR RATIOS TO NET RADIATION BETWEEN THE PRESENT STUDY AND THE RESULT OF KATO AND YAMAGUCHI (2007)

Value Range (W/m^2)	Winter		Summer	
	Present study	Kato & Yamaguchi, 2007	Present study	Kato & Yamaguchi, 2007
	Feb. 6, 2006	Jan. 2, 2004	June 16, 2001	July 10, 2000
Net Radiation (R_n)	250-360	250-310	467-784	530-700
Ground Heat Flux (G)	42-139	N/A	83-292	N/A
Sensible Heat Flux (H)	0-190	0-160	0-313	0-300
Latent Heat Flux (LE)	0-207	0-60	0-479	0-440
H/R_n	urban: 0.39	urban: 0.08; residential: 0.3	urban: 0.28; agriculture: 0.14	urban, 0.2; residential, 0.34; field, 0.14; paddy, 0.05
LE/R_n	urban: 0.18	urban: 0.0; residential: 0.0	urban: 0.23; agriculture: 0.39	urban: 0.0; residential: 0.02; field: 0.27; paddy: 0.37
G/R_n (the reference data may be $\Delta G/R_n$)	urban: 0.4;	urban: 0.91; residential: 0.7	urban: 0.4; agriculture: 0.3	urban: 0.8; residential: 0.64; field: 0.59; paddy: 0.58

Note: The LULC classification scheme for the present study is different from that of Kato and Yamaguchi (2007). In this study, six LULC types, including agricultural land, aquatic systems, barren land, developed land, forest land, and grassland, were identified. Kato and Yamaguchi (2007) identified fifteen LULC types, including tall tree/forest, low tree, orchard, dense grass/paddy field, sparse grass/field, lawn, bare soil/fallow, river/lake, flat pavement, road, industrial area, low-rise dwelling, mid-/high-rise dwelling, commercial/business area, and low-rise building.

Because of the assumption that Kato and Yamaguchi [3] made, their LE/R_n ratio was always zero for the urban category. The present study generated a LE/R_n ratio of 0.18 in February and 0.23 in June for urban. These values were more reasonable based on the fact our "urban" class may contain 30–90% of impervious surfaces and 70–10% of vegetation, water and/or others. As a matter of fact, the *in situ* field observation data with which Kato and Yamaguchi's study were compared showed a LE/R_n ratio of 0.04–0.21 for urban and 0.1–0.3 for residential, a better match with our data. In agricultural areas, the two studies produced a similar LE/R_n ratio. But the present study matched better with paddy field, another type of agricultural land in Japan. This was largely due to their close crop calendars and similar vegetation and moisture conditions. We checked the precipitation record before the acquisition time of the satellite image, and found that there was 25.7 mm on June 16, 2001 (record read at 11:55 AM). This amount of precipitation made cropland in Indiana match better with paddy field in Nagoya, Japan.

Compared with the present study, the G/R_n ratio reported by Kato and Yamaguchi [3] was much higher. They attributed the high ratio to the under-estimation of latent heat. The present study yielded a G/R_n ratio of 0.4 in urban for both the February and June images, and 0.3 in agriculture in June. The *in situ* field observation data with which Kato and Yamaguchi's study was compared displayed a G/R_n ratio of 0.27–0.58 in urban, 0.26–0.74 in residential, and 0.15 in vegetation (grassland and crop). Apparently, the present study was largely in agreement with those *in situ* measurements if we considered that our "urban" class included both their "urban" and "residential". The discrepancy in G/R_n ratio in agriculture may be attributed to the differences in crop type, practice, calendar, and soil moisture conditions. In addition, Kato and Yamaguchi [3] may have combined ground heat flux and anthropogenic heat discharge when computing the storage heat flux (ΔG), and therefore enlarged the value of $\Delta G/R_n$ ratio. We concluded that the compositional ratios of heat fluxes for chosen LULC types in this study were comparable to those of Kato and Yamaguchi [3] and that in some cases we produced better results in reference to the *in situ* measurements examined in Kato and Yamaguchi's study.

Analysis of extreme values of heat fluxes can help to assess the validity of modeling procedures. It is found that a few very low values (0.5% – 1% of the pixels depending on season) existed in the R_n images for all dates. Most of the extreme values of R_n occurred in the urban areas, in particular, in commercial, industrial areas, and the airport area. These areas exhibited both very high surface temperature and albedo, which led to relatively low values in R_n. The reason for the extreme values of net radiation may be the heterogeneity of downward solar radiation and longwave radiation, which is out of the scope of this study. Extreme high values (0.002% – 0.1% of the pixels) were also observed in the estimation of sensible heat flux. Since our model assumed a constant wind speed, extreme values of H may arise because the observed surface temperature may be mismatched with the appropriate wind speed. Some of the extreme H values were associated with image classification errors. Vegetated pixels, for instance, when misclassified as urban, which was associated with higher surface temperatures, would result in extreme high values in H. Moreover, the extreme high values in H were discovered in industrial areas. Within these industrial areas, a huge amount of energy consumption was transferred into atmosphere as sensible heat. In contrast, extreme high values (0.13% – 1.9% of the pixels) in latent heat flux were detected mostly from water bodies. Water bodies generally had high values of LE due to their low temperatures as a result of evaporation.

IV. DISCUSSION

This study has approached urban surface energy balance using TSEB. This approach maximized the use of satellite data from a multispectral remote sensing, in conjunction with a minimum amount of routine meteorological data from a permanent weather station. We realized that meteorological data from an observational network, if available, would certainly improve the modeling results. Atmospheric temperatures, for example, were used for estimation of R_n, H, and LE at the pixel level. More point-based observations of air temperature would allow for the use of various spatial interpolation algorithms to generate a temperature surface to match with the chosen pixel size of satellite imagery. Such data would strongly enhance the estimation of spatially distributed heat fluxes. Similarly, we found that the estimation of sensible heat flux was rather sensitive to the wind speed. More point-based observations of

wind speed would allow for a more accurate estimation of the aerodynamic resistance and thus sensible heat flux.

In estimating sensible heat flux, the temperature of the source for the convective heat transfer, often denoted as T_0, must be known. It can be determined from the profiles of temperature and wind speed in the boundary layer [49]. For an aerodynamically smooth surface, T_0 and T_B, the directional brightness temperature (temperature derived from the inversion of Plank's law for a thermal sensor operating in a given waveband – [50]) are equivalent, since a surface is the source for both the radiative and convective or sensible heat flux [15]. However, most earth's surfaces are not smooth, especially in the urban areas, T_0 and T_B are not equivalent [51], [52]. Since T_0 is difficult to obtain from a remote sensor, this study replaced T_0 with T_s in (8), while replaced T_c with T_s in (9). T_s is equivalent to directional radiometric temperature, a term by Voogt and Oke [50], to indicate temperature that has been corrected for atmospheric transmission and surface emissivity effects. It is suggested that the use of radiometric temperatures for calculating sensible heat flux should incorporate an extra resistance as indicated by (8) [42], [53].

A TSEB model was used in this study. The H for the vegetated and non-vegetated areas was calculated separately following different procedures. Accurate estimation of vegetation fraction should be practiced to avoid over- or under-estimation of heat fluxes. For example, if soil were misclassified as vegetation, the estimated LE would be higher than it should be. On the contrary, if vegetation was misclassified as non-vegetation, an under-estimation of LE would occur. The accuracy of the vegetation fraction needs to be checked against the reference data, e.g., using high resolution aerial photos and/or field work.

Accurate estimation of anthropogenic heat discharge is difficult due to many factors involved. It has been roughly estimated based on the number of vehicles, the energy consumption of buildings, and the energy produced by metabolism [54]. Kato and Yamaguchi [2] proposed to separate H due to anthropogenic heat discharge from H due to radiant heat balance based on some assumptions on R_n, LE, and G, and the residual of the radiant heat balance. Although this study did not estimate anthropogenic heat discharge, it could be estimated in future work using factors such as household energy consumption, night light, traffic density, population density, the number of buildings, and the type of industrial activities, some of which lend themselves to assessment by remote sensing [55]. Recently, Zhou *et al.* [56] developed a simulation model to estimate energy usage of each building with the Department of Energy/ Energy Information Administration survey data, GIS and remotely sensed data.

V. Conclusions

This study has applied a method to study urban surface energy balance using a TSEB approach. This method maximized the use of satellite data from a multispectral remote sensor (i.e., ASTER) in conjunction with a minimum amount of routine meteorological data from a permanent weather station. ASTER images acquired in four distinct seasons were used to derive LULC, LST, vegetation fraction, broadband albedo, broadband emissivity, NDVI, and LAI. Although aerodynamic parameters such as displacement height and roughness length were empirically estimated, they were also computed based on remote sensing data. By applying the method to Marion County, Indiana, U.S.A., this paper has examined the spatial variability of surface heat fluxes in four dates of distinct seasons, as well as the influence of aerodynamic parameters on the estimation of heat fluxes.

Knowledge of urban surface energy balance is fundamental to understanding of UHIs and urban thermal behavior [48], [57]. The main contribution of this study lies in improving the knowledge of the intra-urban variability of surface heat fluxes. Satellite remote sensing imagery and routine meteorological data were integrated for use to provide "snapshots" of spatially-distributed energy fluxes at 90-m resolution. By computing the energy fluxes by LULC type, we can improve understating of the geographical patterns of energy fluxes. Further, the within-class variability was examined with respect to seasonality, and was related to the changes in biophysical variables in addition to the heterogeneity of wind speed and air temperature.

Lacking field data for validation, our estimations of heat fluxes were compared with that of Kato and Yamaguchi [3], which had been verified with *in situ* field measurements. However, surface heat fluxes estimated at this resolution level (90 m) would be more easily validated against ground measurements and helpful for assimilation into more complex simulation models [38]. Remote sensing data can be used to provide "snapshots" of spatially-distributed heat fluxes, which, in turn, can be used to model urban thermal landscape processes as a function of both time and space. The methodology developed in this study by the integration of remotely sensed and routinely measured meteorological data has the advantage of being quite "data-driven" and no need to be calibrated for a particular study site. This methodology would be very helpful for analyzing and modeling UHIs as a result of urbanization-associated LULC and global climate changes.

References

[1] W. G. M. Bastiaanssen, M. Menenti, R. A. Feddes, and A. A. M. Holtslag, "A remote sensing surface energy balance algorithm for land (SEBAL) – 1. Formulation," *J. Hydrol.*, vol. 213, pp. 198–212, 1998.

[2] S. Kato and Y. Yamaguchi, "Analysis of urban heat-island effect using ASTER and ETM+ Data: Separation of anthropogenic heat discharge and natural heat radiation from sensible heat flux," *Remote Sens. Environ.*, vol. 99, pp. 44–54, 2005.

[3] S. Kato and Y. Yamaguchi, "Estimation of storage heat flux in an urban area using ASTER data," *Remote Sens. Environ.*, vol. 110, pp. 1–17, 2007.

[4] T. R. Oke, R. A. Spronken-Smith, E. Jauregui, and C. S. B. Grimmond, "The energy balance of central Mexico City during the dry season," *Atmospheric Environment*, vol. 33, pp. 3919–3930, 1999.

[5] W. J. Timmermans, W. P. Kustas, M. C. Anderson, and A. N. French, "An intercomparison of the Surface Energy Balance Algorithm for Land (SEBAL) and the Two-Source Energy Balance (TSEB) modeling schemes," *Remote Sens. Environ.*, vol. 108, pp. 369–384, 2007.

[6] J. A. Arnfield, "Two decades of urban climate research: A review of turbulence, exchanges of energy and water, and the urban heat island," *Int. J. Climatol.*, vol. 23, pp. 1–26, 2003.

[7] C. S. B. Grimmond, "Progress in measuring and observing the urban atmosphere," *Theoret. Appl. Climatol.*, vol. 84, pp. 3–22, 2006.

[8] A. Martilli, "Current research and future challenges in urban mesoscale modeling," *Int. J. Climatol.*, vol. 27, pp. 1909–1918, 2007.

[9] G. Rigo and E. Parlow, "Modelling the ground heat flux of an urban area using remote sensing data," *Theoret. Appl. Climatol.*, vol. 90, pp. 185–199, 2007.

[10] C. M. Frey, E. Parlow, R. Vogt, M. Harhash, and M. M. A. Wahab, "Flux measurements in Cairo. Part 1: In situ measurements and their applicability for comparison with satellite data," *Int. J. Climatol.*, vol. 31, pp. 218–231, 2011.

[11] J. R. Jensen and D. C. Cowen, "Remote sensing of urban/suburban infrastructure and socioeconomic attributes," *Photogramm. Eng. Remote Sens.*, vol. 65, pp. 611–622, 1999.

[12] Q. Weng, "Remote sensing of impervious surfaces in the urban areas: Requirements, methods, and trends," *Remote Sens. Environ.*, vol. 117, pp. 34–49, 2012.

[13] Q. Weng, "Thermal infrared remote sensing for urban climate and environmental studies: Methods, applications, and trends," *ISPRS J. Photogramm. Remote Sens.*, vol. 64, pp. 335–344, 2009.

[14] D. A. Quattrochi and J. C. Luvall, "Thermal infrared remote sensing for analysis of landscape ecological processes: Methods and applications," *Landscape Ecol.*, vol. 14, pp. 577–598, 1999.

[15] T. J. Schmugge, W. P. Kustas, and K. S. Humes, "Monitoring land surface fluxes using ASTER observations," *IEEE Trans. Geosci. Remote Sens.*, vol. 36, pp. 1421–1430, 1998.

[16] K. Humes, R. Hardy, and W. P. Kustas, "Spatial patterns in surface energy balance components derived from remotely sensed data," *The Professional Geographer*, vol. 52, pp. 272–288, 2000.

[17] K. Wang and S. Liang, "Evaluation of ASTER and MODIS land surface temperture and emissivity products using long-term surface longwave radiation observations at SURFRAD sites," *Remote Sens. Environ.*, vol. 113, pp. 1556–1565, 2009.

[18] K. P. Czajkowski, S. Goward, S. J. Stadler, and A. Walz, "Thermal remote sensing of near surface environmental variables: Application over the Oklahoma mesonet," *The Professional Geographer*, vol. 52, pp. 345–357, 2000.

[19] W. P. Kustas, J. M. Norman, T. J. Schmugge, and M. C. Anderson, "Mapping surface energy fluxes with radiometric temperature," in *Thermal Remote Sensing in Land Surface Processes*, D. A. Quattrochi and J. C. Luvall, Eds. Boca Raton, FL, USA: Taylor and Francis Group, LLC, CRC Press, 2004, pp. 205–253.

[20] A. N. French, D. J. Hunsaker, T. R. Clarke, G. J. Fitzgerald, and P. J. Pinter, "Combining remotely sensed data and ground-based radiometers to estimate crop cover and surface temperatures at daily time steps," *J. Irrigation and Drainage Eng.*, vol. 136, pp. 232–239, 2010.

[21] T. N. Carlson, J. K. Dodd, S. G. Benjamin, and J. N. Cooper, "Satellite estimation of the surface energy balance, moisture availability and thermal inertia," *J. Appl. Meteorol.*, vol. 20, pp. 67–87, 1981.

[22] X. Zhang, Y. Aono, and N. Monji, "Spatial variability of urban surface het fluxes estimated from Landsat TM data under summer and winter conditions," *J. Agricult. Meteorol.*, vol. 54, pp. 1–11, 1998.

[23] J. Hafner and S. Q. Kidder, "Urban heat island modeling in conjunction with satellite-derived surface/soil parameters," *J. Appl. Meteorol.*, vol. 38, pp. 448–465, 1999.

[24] N. Chrysoulakis, "Estimation of the all-wave urban surface radiation balance by use of ASTER multispectral imagery and in situ spatial data," *J. Geophys. Res.*, vol. 108, p. 4582, 2003.

[25] A. R. Gillespie, S. Rokugawa, T. Matsunaga, J. S. Cothern, S. J. Hook, and A. B. Kahle, "A temperature and emissivity separation algorithm for advanced spaceborne thermal emission and reflection radiometer (ASTER) images," *IEEE Trans. Geosci. Remote Sens. E*, vol. 36, pp. 1113–1126, 1998.

[26] S. Liang, "Narrowband to broadband conversions of land surface albedo I: Algorithms," *Remote Sens. Environ.*, vol. 76, pp. 213–238, 2000.

[27] K. Ogawa, T. Schmugge, F. Jacob, and A. French, "Estimation of land surface window (8–12 μm) emissivity from multispectral thermal infrared remote sensing–A case study in a part of Sahara Desert," *Geophys. Res. Lett.*, vol. 30, p. 1067, 2003.

[28] Q. Weng, X. Hu, and H. Liu, "Estimating impervious surfaces using linear spectral mixture analysis with multi-temporal ASTER images," *Int. J. Remote Sens.*, vol. 30, pp. 4807–4830, 2009.

[29] Q. Weng, H. Liu, B. Liang, and D. Lu, "The spatial variations of urban land surface temperatures: Pertinent factors, zoning effect, and seasonal variability," *IEEE J. Sel. Topics Appl. Earth Observ. Remote Sens. (JSTARS)*, vol. 1, pp. 154–166, 2008.

[30] W. H. Brutsaert, *Evaporation Into the Atmosphere: Theory, History and Applications*. London, U.K.: D. Reidel Publishing Co., 1982, p. 299.

[31] J. C. Milder, "ASTER Processing Method," Dept. Natural Resources, Cornell Univ., 2012 [Online]. Available: https://sharepoint.ngdc.wvu.edu/sites/digital_soils/Remote%20Sensing/Models/ASTER_processing_method_FINAL_7-25-08.doc

[32] K. Anandakumar, "A study on the partition of net radiation into heat fluxes on a dry asphalt surface," *Atmosph. Environ.*, vol. 33, pp. 3911–3918, 1999.

[33] R. Silberstein, A. Held, T. Hatton, N. Viney, and M. Sivapalan, "Energy balance of a natural jarrah (Eucalyptus marginata) forest in Western Australia: Measurements during the spring and summer," *Agricult. Forest Meteorol.*, vol. 109, pp. 79–104, 2001.

[34] J. A. Santanello Jr. and M. A. Friedl, "Diurnal covariation in soil heat flux and net radiation," *J. Appl. Meteorol.*, vol. 42, pp. 851–862, 2003.

[35] C. S. B. Grimmond, H. A. Cleugh, and T. R. Oke, "An objective urban heat storage model and its comparison with other schemes," *Atmosph. Environ.*, vol. 25, pp. 311–326, 1991.

[36] W. P. Kustas and J. M. Norman, "Evaluation of soil and vegetation heat flux predictions using a simple two-source model with radiometric temperatures for partial canopy cover," *Agricult. Forest Meteorol.*, vol. 94, pp. 13–29, 1999.

[37] S. M. Liu, L. Lu, D. Mao, and L. Jia, "Evaluating parameterizations of aerodynamic resistance to heat transfer using field measurements," *Hydrol. Earth Syst. Sci.*, vol. 11, pp. 769–783, 2007.

[38] K. Humes, R. Hardy, W. P. Kustas, J. Prueger, and P. Starks, "High spatial resolution mapping of surface energy balance components with remotely sensed data," in *Thermal Remote Sensing in Land Surface Processes*, D. A. Quattrochi and J. C. Luvall, Eds. Boca Raton, FL, USA: Taylor and Francis Group, LLC, CRC Press, 2004, pp. 110–132.

[39] H. P. Schmid, H. A. Cleugh, C. S. B. Grimmond, and T. R. Oke, "Spatial variability of energy fluxes in suburban terrain," *Boundary-Layer Meteorology*, vol. 54, pp. 249–276, 1991.

[40] J. H. Prueger, W. P. Kustas, L. E. Hipps, and J. L. Hatfield, "Aerodynamic parameters and sensible heat flux estimates for a semi-arid ecosystem," *J. Arid Environments*, vol. 57, pp. 87–100, 2004.

[41] G. S. Campbell and J. M. Norman, *An Introduction to Environmental Biophysics*. New York, NY, USA: Springer-Verlag, 1998.

[42] M. Kanda, M. Kanega, T. Kawai, R. Moriwaki, and H. Sugawara, "Roughness lengths for momentum and heat derived from outdoor urban scale models," *J. Appl. Meteorol. Climatol.*, vol. 46, pp. 1067–1079, 2007.

[43] R. W. Macdonald, R. F. Griffiths, and D. J. Hall, "An improved method for estimation of surface roughness of obstacle arrays," *Atmospheric Environment*, vol. 32, pp. 1857–1864, 1998.

[44] W. P. Kustas, A. N. French, J. L. Hatfield, T. J. Jackson, M. S. Moran, A. Rango, J. C. Ritchie, and T. J. Schmugge, "Remote sensing research in hydrometeorology," *Photogramm. Eng. Remote Sens.*, vol. 69, pp. 631–646, 2003.

[45] S. J. Burian, W. S. Han, and M. J. Brown, "Morphological Analyses Using 3D Building Databases," Los Alamos National Lab., Houston, TX, USA, LA-UR-03-8633, 2003.

[46] C. S. B. Grimmond and T. R. Oke, "Aerodynamic properties of urban areas derived from analysis of surface form," *J. Appl. Meteorol.*, vol. 38, pp. 1262–1292, 1999.

[47] M. R. Raupach, "Simplified expressions for vegetation roughness length and zero-plane displacement as functions of canopy height and area index," *Boundary-Layer Meteorology*, vol. 71, pp. 211–216, 1994.

[48] T. R. Oke, "The urban energy balance," *Progress in Physical Geography*, vol. 12, pp. 471–508, 1988.

[49] N. D. S. Huband and J. L. Monteith, "Radiative surface temperature and energy balance of a wheat canopy: I. Comparison of radiative and aerodynamic canopy temperatures," *Boundary-Layer Meteorology*, vol. 36, pp. 1–17, 1986.

[50] J. A. Voogt and T. R. Oke, "Thermal remote sensing of urban climates," *Remote Sens. Environ.*, vol. 86, pp. 370–384, 2003.

[51] F. G. Hall, K. F. Huemmrich, P. J. Sellers, and J. E. Nickeson, "Satellite remote sensing of surface energy balance: Success, failures, and unresolved issues in FIFE," *J. Geophys. Res.*, vol. 97, pp. 19061–19089, 1992.

[52] J. M. Norman, M. Divakarla, and N. S. Goel, "Algorithms for extracting information from remote thermal-IR observations of the earth's surface," *Remote Sens. Environ.*, vol. 51, pp. 157–168, 1995.

[53] J. A. Voogt and C. S. B. Grimmond, "Modeling surface sensible heat flux using surface radiative temperatures in a simple urban area," *J. Appl. Meteorol.*, vol. 39, pp. 1679–1699, 2000.
[54] D. J. Sailor and L. Lu, "A top-down methodology for developing diurnal and seasonal anthropogenic heating profiles for urban areas," *Atmospheric Environment*, vol. 38, pp. 2737–2748, 2004.
[55] D. J. Sailor, "A review of methods for estimating anthropogenic heat and moisture emissions in the urban environment," *Int. J. Climatol.*, vol. 31, pp. 189–199, 2010.
[56] Y. Y. Zhou, Q. Weng, K. R. Gurney, Y. Shuai, and X. Hu, "Estimation of the relationship between remotely sensed anthropogenic heat discharge and building energy use," *ISPRS J. Photogramm. Remote Sens.*, vol. 67, pp. 65–72, 2012.
[57] T. R. Oke, "The energetic basis of the urban heat island," *Quart. J. Royal Meteorol. Soc.*, vol. 108, pp. 1–24, 1982.

Qihao Weng (M'07) was born in Fuzhou, China. He received the A.S. diploma in geography from Minjiang University, China, in 1984, the M.S. degree in physical geography from South China Normal University, Guangzhou, China, in 1990, the M.A. degree in geography from the University of Arizona, Tucson, AZ, USA, in 1996, and the Ph.D. degree in geography from the University of Georgia, Athens, GA, USA, in 1999.

He is currently a Professor of geography and Director of the Center for Urban and Environmental Change, Indiana State University, Terre Haute, IN, USA. During 2008–2009, he visited NASA Marshall Space Flight Center as a senior research fellow. He is the author of more than 150 publications and 8 books. He serves as an Associate Editor of *ISPRS Journal of Photogrammetry and Remote Sensing*, and is the series editor for the *Taylor & Francis Series in Remote Sensing Applications*. His research focuses on remote sensing and GIS analysis of urban ecological and environmental systems, land-use and land-cover change, urbanization impacts, and human-environment interactions.

Dr. Weng is a member of ASPRS and AAG. He is the Coordinator for GEO's SB-04, Global Urban Observation and Information Task (2012–15), and served as a National Director of the American Society for Photogrammetry and Remote Sensing (2007–2010). He was the 2011 recipient of the Outstanding Contributions Award in Remote Sensing sponsored by American Association of Geographers (AAG) Remote Sensing Specialty Group, the first-place recipient of the Erdas Award for Best Scientific paper in Remote Sensing (2010) and the recipient of the Robert E. Altenhofen Memorial Scholarship Award, both from the American Society for Photogrammetry and Remote Sensing (1999), and the Best Student-Authored Paper Award from the International Geographic Information Foundation (1998). In 2006, he received the Theodore Dreiser Distinguished Research Award from Indiana State University, the university's highest research honor bestowed to faculty. In 2008, he was awarded a senior fellowship from NASA.

Xuefei Hu received the B.S. and M.S. degrees from the China University of Geosciences, Beijing, China, and the Ph.D. degree from Indiana State University, Terre Haute, IN, USA.

He is currently a research associate at the Rollins School of Public Health, Emory University, Atlanta, GA, USA. His research interests focus on the estimation of impervious surface from remote sensing imageries, artificial neural networks, geographic information systems, and the use of geospatial technologies for environmental health studies.

Dale A. Quattrochi received the Ph.D. degree from the University of Utah, Salt Lake City, UT, USA, the M.S. degree from the University of Tennessee, Knoxville, TN, USA, and the B.S. degree from Ohio University, Athens, OH, USA, all in geography.

He is a Senior Research Scientist with the NASA Marshall Space Flight Center, Huntsville, AL, USA, and has over 30 years of experience in the field of Earth science remote sensing research and applications. His research interests focus on the application of thermal remote sensing data for analysis of heating and cooling patterns across the diverse urban landscape as they impact the overall local and regional environment. He is also conducting research on the applications of geospatial statistical techniques, such as fractal analysis, to multiscale remote sensing data. He is the co-editor of two books: *Scale in Remote Sensing and GIS* (with Michael Goodchild) published in 1997 by CRC/Lewis Publishers, and *Thermal Remote Sensing in Land Surface Processes* (with Jeffrey Luvall) published in 2004 by CRC Press.

Dr. Quattrochi is the recipient of numerous awards including the NASA Exceptional Scientific Achievement Medal, NASA's highest science award, which he received for his research on urban heat islands and remote sensing. He is also a recipient of the Ohio University College of Arts and Science, Distinguished Alumni Award.

Hua Liu received the B.A. degree in computer-aided cartography from Wuhan Technical University of Surveying and Mapping, China, in 2000, the M.A. degree in cartography and GIS from Wuhan University in 2003, and the Ph.D. degree in physical geography from Indiana State University, Terre Haute, IN, USA, in 2007.

She is currently an Assistant Professor at the College of Arts and Letters, Old Dominion University, Norfolk, VA, USA. Her research focuses on urban thermal behaviors, landscape pattern, and GIS and remote sensing applications in public health.